Article

Analysis of Proton–Proton Transfer Dynamics in Rotating Solids and Their Use for 3D Structure Determination

Adam Lange, Karsten Seidel, Laurent Verdier, Sorin Luca, and Marc Baldus

J. Am. Chem. Soc., **2003**, 125 (41), 12640-12648• DOI: 10.1021/ja034555g • Publication Date (Web): 18 September 2003

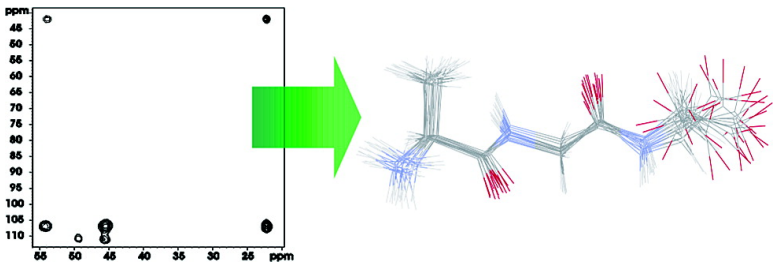

More About This Article

Additional resources and features associated with this article are available within the HTML version:

- Supporting Information
- Links to the 16 articles that cite this article, as of the time of this article download
- Access to high resolution figures
- Links to articles and content related to this article
- Copyright permission to reproduce figures and/or text from this article

View the Full Text HTML

J|A|C|S
ARTICLES
Published on Web 09/18/2003

Analysis of Proton−Proton Transfer Dynamics in Rotating Solids and Their Use for 3D Structure Determination

Adam Lange, Karsten Seidel, Laurent Verdier, Sorin Luca, and Marc Baldus*

Contribution from the Max-Planck-Institute for Biophysical Chemistry, Department of NMR-Based Structural Biology, 37077 Göttingen, Germany

Received February 7, 2003; E-mail: maba@mpibpc.mpg.de

Abstract: A detailed analysis of proton−proton-transfer dynamics under magic angle spinning NMR is presented. Results obtained on model compounds are evaluated under different experimental conditions and NMR mixing schemes. It is shown that the resulting buildup rates can be interpreted in terms of internuclear proton−proton distances provided that an appropriate theoretical description is chosen. As demonstrated in two test applications, these dependencies can be used in the context of a three-dimensional structure determination in the solid state.

Introduction

Solid-state nuclear magnetic resonance (NMR) has recently made considerable progress in providing structural information in systems such as surface bound peptides,[1] membrane,[2,3] or fibrous[4,5] proteins that are difficult to study by solution-state NMR or X-ray crystallography. The vast majority of these studies (for recent reviews, see refs 6 and 7) involve NMR-sensitive nuclei such as ^{13}C or ^{15}N, for which nontrivial structural information from through-space dipolar couplings is only obtainable by advanced labeling approaches[8] and/or by the application of specifically designed NMR pulse schemes.[9−11] In a uniformly labeled polypeptide, (^{13}C,^{13}C) or (^{13}C,^{15}N) distance constraints between 3 and 6 Å which are of central importance for defining backbone and side chain conformation, have thus far only been determined using chemical shift selective transfer methods.[9] In this case, each individual distance constraint necessitated the recording of at least one NMR data set. Even in small peptides, the complete 3D structural characterization can hence require a considerable number of NMR experiments making structural investigations in larger systems impractical.

In contrast to structural studies involving rare-spin nuclei,[12] even the strongest (^1H,^1H) contacts provide valuable structural details and, in many cases, lead to a remarkably accurate description of the three-dimensional fold of the molecule of interest.[13] It is hence not surprising that biomolecular structure determination by solution-state NMR relies profoundly on the detection of short (<5Å) proton−proton distance restraints[13−15] which can be identified with considerable reliability.[13,16−18] Here, a variety of radio frequency (r.f.) mixing schemes (including NOESY[14,17,19] or ROESY[20] experiments) are available to simultaneously detect a large set of (^1H,^1H) contacts as cross-peak intensities within a standard multidimensional correlation experiment.

(1) Long, J. R.; Oyler, N.; Drobny, G. P.; Stayton, P. S. *J. Am. Chem. Soc.* **2002**, *124*, 6297−6303.
(2) Smith, S. O.; Song, D.; Shekar, S.; Groesbeek, M.; Ziliox, M.; Aimoto, S. *Biochemistry* **2001**, *40*, 6553−6558; Isaac, B.; Gallagher, G. J.; Balazs, Y. S.; Thompson, L. K. *Biochemistry* **2002**, *41*, 3025−3036.
(3) Luca, S.; White, J. F.; Sohal, A. K.; Filipov, D. V.; van Boom, J. H.; Grisshammer, R.; Baldus, M. *Proc. Natl. Acad. Sci. U.S.A.* **2003**, *100*, 10 706−10 711.
(4) van Beek, J. D.; Hess, S.; Vollrath, F.; Meier, B. H. *Proc. Natl. Acad. Sci. U.S.A.* **2002**, *99*, 10 266−10 271.
(5) Petkova, A. T.; Ishii, Y.; Balbach, J. J.; Antzutkin, O. N.; Leapman, R. D.; Delaglio, F.; Tycko, R. *Proc. Natl. Acad. Sci.* **2002**, *99*, 16 742−16 747; Jaroniec, C. P.; MacPhee, C. E.; Astrof, N. S.; Dobson, C. M.; Griffin, R. G. *Proc. Natl. Acad. Sci.* **2002**, *99*, 16 748−16 753.
(6) Griffin, R. G. *Nat. Struct. Biol.* **1998**, *5*, 508−512; Tycko, R. *Curr. Opin. Chem. Biol.* **2000**, *4*, 500−506; Thompson, L. K. *Curr. Opin. Struct. Biol.* **2002**, *12*, 661−669.
(7) Baldus, M. *Prog. Nucl. Magn. Reson. Spectrosc.* **2002**, *41*, 1−47.
(8) Smith, S. O.; Aschheim, K.; Groesbeek, M. *Q. Rev. Biophys.* **1996**, *29*, 395−449; LeMaster, D. M.; Kushlan, D. M. *J. Am. Chem. Soc.* **1996**, *118*, 9255−9264; Gardner, K. H.; Kay, L. E. *Annu. Rev. Biophys. Biomolec. Struct.* **1998**, *27*, 357−406; Hong, M.; Jakes, K. *J. Biomol. NMR* **1999**, *14*, 71−74; Castellani, F.; van Rossum, B.; Diehl, A.; Schubert, M.; Rehbein, K.; Oschkinat, H. *Nature* **2002**, *420*, 98−102.
(9) Nomura, K.; Takegoshi, K.; Terao, T.; Uchida, K.; Kainosho, M. *J. Am. Chem. Soc.* **1999**, *121*, 4064−4065; Rienstra, C. M.; Tucker-Kellogg, L.; Jaroniec, C. P.; Hohwy, M.; Reif, B.; McMahon, M. T.; Tidor, B.; Lozano-Perez, T.; Griffin, R. G. *Proc. Natl. Acad. Sci. U.S.A.* **2002**, *99*, 10 260−10 265.
(10) Baldus, M.; Petkova, A. T.; Herzfeld, J.; Griffin, R. G. *Mol. Phys.* **1998**, *95*, 1197−1207.
(11) Jaroniec, C. P.; Lansing, J. C.; Tounge, B. A.; Belenky, M.; Herzfeld, J.; Griffin, R. G. *J. Am. Chem. Soc.* **2001**, *123*, 12 929−12 930.
(12) Baldus, M.; Meier, B. H. *J. Magn. Reson.* **1997**, *128*, 172−193; Kiihne, S.; Mehta, M. A.; Stringer, J. A.; Gregory, D. M.; Shiels, J. C.; Drobny, G. P. *J. Phys. Chem. A* **1998**, *102*, 2274−2282; Bennett, A. E.; Rienstra, C. M.; Griffiths, J. M.; Zhen, W. G.; Lansbury, P. T.; Griffin, R. G. *J. Chem. Phys.* **1998**, *108*, 9463−9479; Kiihne, S. R.; Geahigan, K. B.; Oyler, N. A.; Zebroski, H.; Mehta, M. A.; Drobny, G. P. *J. Phys. Chem. A* **1999**, *103*, 3890−3903; Goobes, G.; Boender, G. J.; Vega, S. *J. Magn. Reson.* **2000**, *146*, 204−219; Helluy, X.; Marichal, C.; Sebald, A. *J. Phys. Chem. B* **2000**, *104*, 2836−2845; Goobes, G.; Vega, S. *J. Magn. Reson.* **2002**, *154*, 236−251.
(13) Wüthrich, K. *NMR of Proteins and Nucleic Acids*; Wiley-Interscience: New York, 1986.
(14) Ernst, R. R.; Bodenhausen, G.; Wokaun, A. *Principles of Nuclear Magnetic Resonance in One and Two Dimensions*; Clarendon Press: Oxford, 1987.
(15) Cavanagh, J., Fairbrother, W. J., Palmer, A. G., Skelton, N. J. *Protein NMR Spectroscopy, Principles and Practice*; Academic Press: San Diego, 1996.
(16) Solomon, I. *Phys. Rev.* **1955**, *99*, 559−565.
(17) Macura, S.; Ernst, R. R. *Mol. Phys.* **1980**, *41*, 95−117.
(18) Kumar, A.; Wagner, G.; Ernst, R. R.; Wuthrich, K. *J. Am. Chem. Soc.* **1981**, *103*, 3654−3658.
(19) Jeener, J.; Meier, B. H.; Bachmann, P.; Ernst, R. R. *J. Chem. Phys.* **1979**, *71*, 4546−4553.
(20) Bothnerby, A. A.; Stephens, R. L.; Lee, J. M.; Warren, C. D.; Jeanloz, R. W. *J. Am. Chem. Soc.* **1984**, *106*, 811−813; Bax, A.; Davis, D. G. *J. Magn. Reson.* **1985**, *63*, 207−213; Griesinger, C.; Ernst, R. R. *J. Magn. Reson.* **1987**, *75*, 261−271.

10.1021/ja034555g CCC: $25.00

Ideally, a similar large set of (^{1}H,^{1}H) distance parameters, read out in a single, 2D correlation experiment, could provide the basis for determining the three-dimensional arrangement of a molecule in the solid-state. Here, the ability to directly detect (^{1}H,^{1}H) contacts is strongly influenced by the residual proton line width. In systems with a limited set of ^{1}H resonances or in the presence of residual internal mobility, line-narrowing techniques such as multiple-pulse decoupling[21] or ultrafast magic angle spinning[22] can be sufficient to probe proton−proton interactions in high spectral resolution. In many biophysical applications, additional complications arise due to the number of ^{1}H resonances to be expected and due to the limited spectral dispersion. For this reason, indirect detection schemes that encode (^{1}H,^{1}H) dipolar couplings on rare-spin nuclei are particularly attractive. They have previously been demonstrated in the context of ^{1}H-spin counting[23,24] and for 2D rare spin correlation spectroscopy.[25−27]

In polypeptides, a variety of nontrivial distance constraints can be detected if ^{15}N or ^{13}C evolution periods are used and if the (^{1}H,^{1}H) mixing time is restricted to the initial rate regime.[26] If constraints obtained from these N/CHHC 2D experiments are to be supplemented in the framework of a de novo three-dimensional structure determination, the transfer intensities must be examined in more detail. In addition, such attempts require a principle understanding of the polarization transfer dynamics within a proton network in the solid-state. As the general driving force of (^{1}H,^{1}H) transfer in the solid-state, dipolar interactions between neighboring proton spins have thus far been described as a deterministic, quantum-mechanical (QM) transfer mechanism[22,23] or as a dissipative spin diffusion process.[28,29] An appropriate theoretical description furthermore not only depends on the details of the (^{1}H,^{1}H) mixing but also on the time scale for which (^{1}H,^{1}H) transfer is allowed to take place. For example, results of mixing times in the order of ms have been analyzed within the concept of a classical exchange process with a uniform diffusion coefficient.[25] As we will show below, a simple extension of this model for shorter mixing times[27] or a QM analysis successfully utilized at ultrafast MAS conditions[22] is not possible in general. Instead, a detailed analysis of the experimental parameters such as the B_0 field, MAS rate, and the type of r.f. mixing scheme is mandatory.

The purpose of our manuscript is hence 2-fold: First, we show that an adequate theoretical analysis of (^{1}H,^{1}H) transfer rates generally depends on the details of the NMR experiment. A comprehensive examination of the transfer dynamics in uniformly labeled model compounds leads to a general framework in which (^{1}H,^{1}H) transfer rates can be related to internuclear distances for the considered proton−proton mixing schemes and MAS rates. In the second part of our contribution, we exemplify how these distance constraints can be utilized in the context of a conventional structure calculation routine to determine the 3D conformation of a uniformly [^{13}C,^{15}N] labeled biomolecule in the solid state.

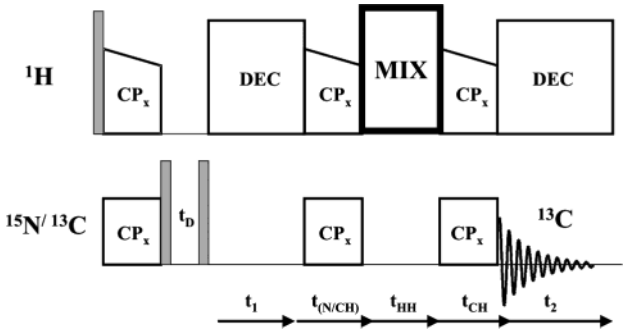

Figure 1. Generic two-dimensional pulse scheme to observe (^{1}H,^{1}H) polarization transfer in two spectral rare-spin dimensions.[26] (^{1}H,^{1}H) contacts are encoded during a two-dimensional (^{15}N,^{13}C) (NHHC) or (^{13}C,^{13}C) (CHHC) correlation experiment. Further experimental details are given in ref 26.

Material and Methods

Sample Preparation. U-[^{13}C,^{15}N] labeled samples of L-Valine and L-Histidine·HCl were purchased from Cambridge Isotope Laboratories (CIL, Andover, MA). U-[^{13}C,^{15}N] labeled Ala-Gly-Gly was chemically synthesized as described previously.[30] L-Histidine·HCl and Ala-Gly-Gly were recrystallized from aqueous solutions at 10% dilution using standard procedures.

NMR Spectroscopy. All NMR experiments were conducted on 9.4 T (^{1}H resonance frequency: 400 MHz) or 14.1 T (^{1}H resonance frequency: 600 MHz) wide-bore instruments (Bruker/Germany) using 2.5 mm and 4 mm triple-resonance (^{1}H,^{13}C,^{15}N) MAS probes. The generic two-dimensional N/CHHC mixing scheme[26] is depicted in Figure 1 and involves rare-spin evolution and detection times. Unless stated otherwise, heteronuclear t_{NH} and t_{CH} contact times were set to 200 and 100 μs, respectively. Phase sensitive 2D spectroscopy was established by means of TPPI phase cycling.[14]

For efficient (^{1}H,^{1}H) transfer, signal loss during the mixing sequence must be minimized. For this purpose, ^{1}H signal intensities of unlabeled Ala-Gly-Gly were recorded under the condition of radio frequency (r.f.) pulse spin-locking and nutation with phase inversion as a function of the ratio of r.f. field and MAS rate $\kappa = \omega_1/\omega_R$. In Figure 2 signal intensities are plotted after an r.f. (spin-lock or nutation) evolution time of 200 μs. For both experimental cases, we observe distinct resonance minima at the higher MAS rate (25 kHz) if $\kappa \in [0.5,1,2]$, in line with results obtained in rare-spin applications.[10,31] For the lower spinning speed (11 kHz), the overall signal pattern is further complicated. For both MAS rates, spin locking is most efficient for the strongest applied r.f. fields (Figure 2a). Signal loss under r.f. nutation (Figure 2c) is minimal for very small or large r.f. fields, and one finds broadened resonance minima around the $\kappa \in [0.5,1,2]$ conditions that narrow with increasing MAS rates. So as to ensure that the experimentally observed signal loss is indeed induced by strong dipolar (^{1}H,^{1}H) couplings, full quantum mechanical simulations within the numerical simulation routine GAMMA[32,33] were carried out (vide infra). Because dipolar (^{1}H,^{1}H) interactions can be of comparable size to the applied MAS rate, a stepwise integration procedure (see e.g., ref 7) of the relevant two-

(21) Caravatti, P.; Braunschweiler, L.; Ernst, R. R. *Chem. Phys. Lett.* **1983**, *100*, 305−310.
(22) Schnell, I.; Spiess, H. W. *J. Magn. Reson.* **2001**, *151*, 153−227.
(23) Zhang, S.; Meier, B. H.; Ernst, R. R. *Phys. Rev. Lett.* **1992**, *69*, 2149−2151.
(24) Tomaselli, M.; Hediger, S.; Suter, D.; Ernst, R. R. *J. Chem. Phys.* **1996**, *105*, 10 672−10 681.
(25) Wilhelm, M.; Feng, H.; Tracht, U.; Spiess, H. W. *J. Magn. Reson.* **1998**, *134*, 255−260; Mulder, F. M.; Heinen, W.; van Duin, M.; Lugtenburg, J.; de Groot, H. J. M. *J. Am. Chem. Soc.* **1998**, *120*, 12 891−12 894.
(26) Lange, A.; Luca, S.; Baldus, M. *J. Am. Chem. Soc.* **2002**, *124*, 9704−9705.
(27) de Boer, I.; Bosman, L.; Raap, J.; Oschkinat, H.; de Groot, H. J. M. *J. Magn. Reson.* **2002**, *157*, 286−291.
(28) Suter, D.; Ernst, R. R. *Phys. Rev. B* **1982**, *25*, 6038−6041; Suter, D.; Ernst, R. R. *Phys. Rev. B* **1985**, *32*, 5608−5627.
(29) Kubo, A.; McDowell, C. A. *J. Chem. Soc. Faraday Trans. I* **1988**, *84*, 3713−3730.
(30) Luca, S.; Filippov, D. V.; van Boom, J. H.; Oschkinat, H.; de Groot, H. J. M.; Baldus, M. *J. Biomol. NMR* **2001**, *20*, 325−331.
(31) Oas, T. G.; Griffin, R. G.; Levitt, M. H. *J. Chem. Phys.* **1988**, *89*, 692−695; Gan, Z. H.; Grant, D. M. *Chem. Phys. Lett.* **1990**, *168*, 304−308; Nielsen, N. C.; Creuzet, F.; Griffin, R. G.; Levitt, M. H. *J. Chem. Phys.* **1992**, *96*, 5668−5677; Verel, R.; Baldus, M.; Ernst, M.; Meier, B. H. *Chem. Phys. Lett.* **1998**, *287*, 421−428.

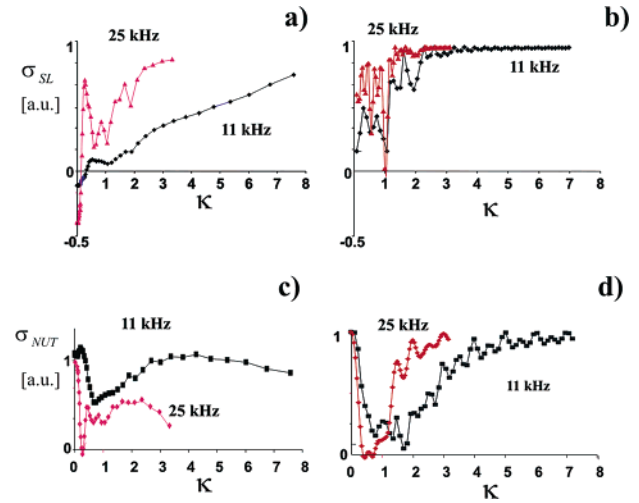

Figure 2. Spin-lock (a,b) and nutation (c,d) behavior of ^{1}H resonances in the tri-peptide AGG for the two indicated MAS rates. Experimental results (a,c) were obtained on a 600 MHz wide-bore (Bruker/Germany) NMR instrument. Numerical simulations of the spin-lock (b) and nutation (d) behavior result from considering a dipolar coupled two-spin system for the two indicated MAS rates. All simulations were obtained using the C++ based NMR simulation environment GAMMA.[32,33] A stepwise integration procedure (see, for example, ref 7) was utilized to calculate the time evolution of the spin system. Results of 1000 single-crystal orientations were added. The total signal intensity after an evolution of 200 μs is shown as a function of $\kappa = \omega_1/\omega_R$.

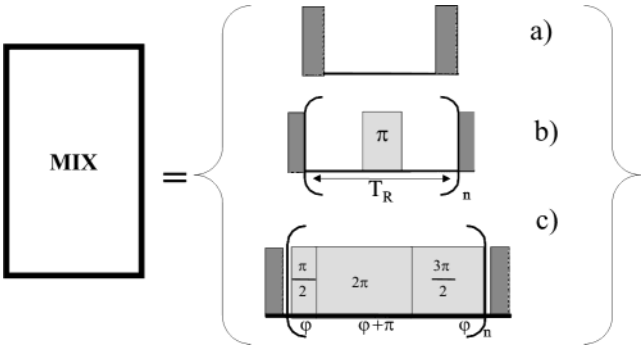

Figure 3. (^{1}H,^{1}H) mixing schemes considered in the current study. (a) relates to longitudinal mixing (LM), (b) to RFDR[35] zero-quantum (0Q) mixing and (c) to POST-C7[36] double-quantum (2Q) mixing. Unless stated otherwise, shaded pulses correspond to the 90° pulse nutations. In (b) and (c), *n* refers to the number of rotor periods T_R and basic POST-C7 cycles, respectively.

spin Hamiltonian was performed (see the Supporting Information). In Figure 2, the spin-lock (b) and nutation (d) behavior predicted for the two MAS rates considered experimentally is shown. Again, the signal intensity was determined after 200 μs of spin system evolution as a function of $\kappa = \omega_1/\omega_R$. In full agreement with our experimental results, favorable spin-lock and nutation behavior is detected for large ratios $\kappa = \omega_1/\omega_R$. Small values of κ are also possible for nutation experiments. In general, the agreement between the theoretical predictions of a homonuclear dipolar coupled two-spin system and the empirical findings is better for ultrafast MAS conditions. A further improvement between simulation and experiment may be obtained by taking into account r.f. inhomogeneity and offset effects or by including additional spins in the QM calculation. The r.f. schemes compatible with our theoretical and experimental results are summarized in Figure 3. Longitudinal mixing (LM) (Figure 3a) fulfills the experimental restrictions obtained from Figure 2. Moreover, polarization transfer schemes that are characterized by relatively high values of κ minimize relaxation effects. For example, SEDRA[34]/RFDR[35] schemes that involve strong, rotor-synchronized π pulses are known to promote homonuclear dipolar recoupling among ^{13}C nuclei. In Figure 3b, the corresponding RFDR implementation of a (^{1}H,^{1}H) mixing experiment is shown. Both LM and RFDR represent laboratory frame mixing schemes and are, as demonstrated below, characterized by zero-quantum polarization transfer. Finally, rotating frame double-quantum schemes that are characterized by large values of κ can be utilized. In Figure 3c, the POST-C7 scheme as published by Hohwy et al.[36] has been adapted.

Theoretical Background. The experimentally detected cross-peak build-up curves were analyzed using three different theoretical models.

(a) Spectral spin diffusion.[28,29] Here, the cross-peak signal intensity is described by an exponential buildup

$$I_{12,z}(t) = 1 - \exp(-t/T_{SD}) \tag{1}$$

In the static case, the spin-diffusion time constant T_{SD} is given by the (^{1}H,^{1}H) distance r_{12} of interest and the zero-quantum (0Q) line-shape function, evaluated at the isotropic chemical shift difference Δ of *I* spin 1 and 2

$$\frac{1}{T_{SD}} = (\mu_0/4\pi)^2 \frac{\hbar^2 \gamma_I^4}{r_{12}^6} J^{0Q}(\Delta) \tag{2}$$

To lowest approximation, eq 2 remains valid under MAS and/or the presence of an r.f. scheme assuming a modified 0Q-line-shape function $J^{0Q.RF}(\Delta,\omega_R)$.[29]

(b) Two-spin approximation. Within the simulation environment GAMMA,[32] a dipolar coupled (^{1}H,^{1}H) two-spin system was monitored under the influence of MAS for all considered r.f. mixing schemes. Isotropic and anisotropic ^{1}H chemical shielding interactions were taken from the literature.[37] The Hamiltonian and the details of the calculation are given as Supporting Information.

(c) We also investigated whether the concept of a standard diffusion coefficient[25] would adequately explain our experimental findings.

Structure Calculation. All structure calculations were performed within CNS[38] (Crystallography and NMR System). (^{1}H,^{1}H) distance restraints obtained from N/CHHC 2D spectra were treated as NOE restraints represented by a square-well potential

$$E_{SSNMR} = \sum k_{HH} \begin{cases} (r_{ij} - r_{ij}^u)^2, & r_{ij} > r_{ij}^u \\ 0, & r_{ij}^l < r < r_{ij}^u \\ (r_{ij} - r_{ij}^l)^2, & r_{ij} < r_{ij}^l \end{cases} \tag{3}$$

where r_{ij} is the calculated distance between proton i and j, r_{ij}^l and r_{ij}^u are the values of the lower and upper limits of the target distances, respectively, and k_{HH} is the force constant. In case of ambiguous (^{1}H,^{1}H) restraints involving methyl or methylene protons, r_{ij} is computed by an r^{-6} summation[39] involving all possible proton−proton contacts. Extended conformers of Ala-Gly-Gly and L-Histidine·HCl were created as initial structures and subsequently subjected to a simulated annealing protocol consisting of three stages:

(32) Smith, S. A.; Levante, T. O.; Meier, B. H.; Ernst, R. R. *J. Magn. Reson. Ser. A* **1994**, *106*, 75−105.
(33) Baldus, M.; Levante, T. O.; Meier, B. H. *Z. Naturfors. Sect. A−J. Phys. Sci.* **1994**, *49*, 80−88.
(34) Gullion, T.; Vega, S. *Chem. Phys. Lett.* **1992**, *194*, 423−428.
(35) Bennett, A. E.; Ok, J. H.; Griffin, R. G.; Vega, S. *J. Chem. Phys.* **1992**, *96*, 8624−8627.
(36) Hohwy, M.; Jakobsen, H. J.; Eden, M.; Levitt, M. H.; Nielsen, N. C. *J. Chem. Phys.* **1998**, *108*, 2686−2694.
(37) Haeberlen, U. In *Advances in Magnetic Resonance*; Academic Press: New York, 1976; Mehring, M. *Principles of High-Resolution NMR in Solids*, 2nd ed.; Springer: Berlin, 1983; Tesche, B.; Haeberlen, U. *J. Magn. Reson. Ser. A* **1995**, *117*, 186−192.
(38) Brunger, A. T.; Adams, P. D.; Clore, G. M.; DeLano, W. L.; Gros, P.; Grosse-Kunstleve, R. W.; Jiang, J. S.; Kuszewski, J.; Nilges, M.; Pannu, N. S.; Read, R. J.; Rice, L. M.; Simonson, T.; Warren, G. L. *Acta Crystallogr. Sect. D-Biol. Crystallogr.* **1998**, *54*, 905−921.
(39) Fletcher, C. M.; Jones, D. N. M.; Diamond, R.; Neuhaus, D. *J. Biomol. NMR* **1996**, *8*, 292−310.

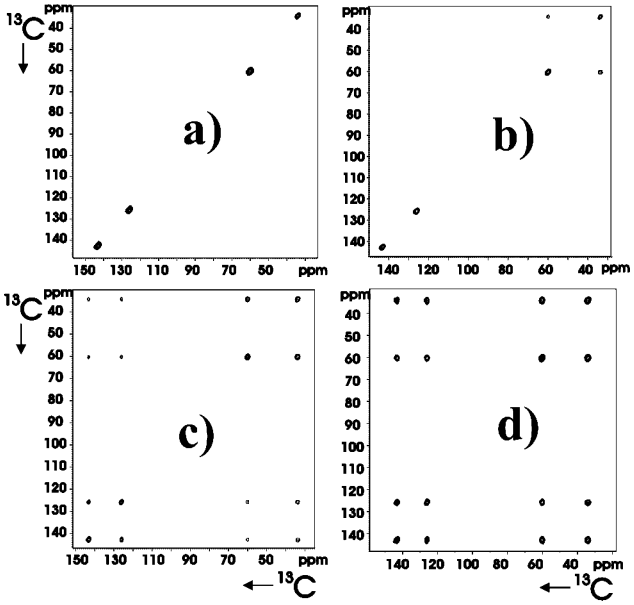

Figure 4. Experimentally observed CHHC cross-peak intensities for His·HCl at 11 kHz on a 400 MHz wide-bore NMR instrument for RFDR mixing (Figure 3b) employing four different mixing times: (a) 0μs, (b) 182 μs, (c) 273 μs, and (d) 364 μs. Cross-peak intensities reflect (^{1}H,^{1}H) interactions, encoded in ^{13}C evolution and detection periods.

L-Histidine·HCl. 1. High-temperature annealing in torsion angle space, in 2000 time steps of 0.002 ps at 30 000 K. 2. Slow-cool annealing stage in torsion angle space, in 6000 steps of 0.002 ps, and temperature reduction from 30 000 K to zero in steps of 250 K. 3. Final conjugate gradient minimization of 300 steps. During all stages, a force constant k_{HH} of 150 kcal mol^{-1} Å^{-2} was used. A set of 100 conformers was generated, starting from different initial velocities.

Ala-Gly-Gly. 1. High-temperature annealing in torsion angle space, in 2000 time steps of 0.005 ps at 50 000 K. 2. Slow-cool annealing stage in torsion angle space, in 4000 steps of 0.005 ps, and temperature reduction from 50 000 K to zero in steps of 250 K. 3. Final conjugate gradient minimization of 200 steps. Force constants k_{HH} of 150 kcal mol^{-1} Å^{-2} were employed during high-temperature and slow-cool annealing, and 75 kcal mol^{-1} Å^{-2} during final minimization.

Dihedral angles derived using TALOS[40] were restrained by harmonic potentials analogous to eq 3 with force constants k of 100, 200, and 400 kcal mol^{-1} rad^{-2} during the three stages, respectively. The RMSDs given by TALOS for each backbone angle were taken as allowed rotations around the predicted angles without energy contribution. Calculations implemented the PROTEIN-ALLHDG[41] parameter file. A set of 50 conformers was generated, starting from different initial velocities. The resulting structures were sorted by total energy and, if applicable, distance and dihedral angle restraint violations.

Results and Discussion

(A) Analysis of Proton−Proton-Transfer Dynamics. Zero-Quantum Mixing. To introduce the general concept of a CHHC 2D correlation experiment, we present in Figure 4 results of a 0Q-CHHC (utilizing the (^{1}H,^{1}H) mixing scheme of Figure 3b) on uniformly [^{13}C,^{15}N] labeled His·HCl at 11 kHz on a 400 MHz instrument. CP times before and after proton mixing were optimized for polarization transfer within CH_x ($x = 1-3$) groups only. The NMR signal of the nonprotonated ring Cγ carbon is correspondingly missing. As expected, we observe no cross-peak intensities for vanishing mixing times (Figure 4a). Increasing the mixing times from 182 μs (Figure 4b) to 0.36 ms (Figure 4d) gradually establishes all (^{13}C,^{13}C) correlations in the side chain spectrum. Because no ^{1}H evolution or detection periods are present, the N/CHHC concept does not allow for the identification of individual (^{1}H,^{1}H) contacts, for example within CH_2 or CH_3 groups. In the following, we will hence refer only to (^{13}C,^{13}C) correlations and tacitly assume that they are mediated by next neighbor proton−proton interactions.

For a further analysis, we present in Figure 5 experimentally observed CHHC cross-peak intensities for a larger set of (LM) transfer times for an MAS rate of 11 kHz (a) and 26 kHz (b). Here, and in all results presented in the following, the cross-peak intensities were normalized against the total intensity of the spectrum. Experimental data points are shown for the pairs Cα−Cβ (filled squares) and Cβ−Cδ (filled diamonds). From neutron diffraction data,[42] (^{1}H, ^{1}H) distances in His·HCl are predicted to be 2.22 Å for the (Cα−Cβ) pair and 3.06 Å for the nearest neighbor (Cβ−Cδ) pair. A simple inspection of Figure 5 reveals that the shorter (^{1}H,^{1}H) distance (i.e., the (Cα−Cβ) pair) is characterized by a significantly faster buildup and, correspondingly, a stronger transfer efficiency in the initial rate regime $t_{HH} = [0, 200\ \mu s]$ in (a) and $t_{HH} = [0, 1000\ \mu s]$ in Figure 5b. Attempts to describe the experimentally detected transfer dynamics within a dipolar coupled two-spin were unsuccessful. Instead, theoretical results shown in Figure 5a and b were obtained using the relaxation analysis of eq 1. Because the (^{1}H,^{1}H) distances are known, we can determine the value of the zero-quantum (0Q) line-shape function and find, for the data obtained at 11 kHz MAS (Figure 5a), $J^{0Q,LM}(\Delta) = 208\ \mu s$. In agreement with a relaxation-based theoretical model, the signal buildup is exponential and the zero-quantum spin diffusion rate under LM mixing scales inversely with the 6th power of the internuclear (^{1}H,^{1}H) distance. In Figure 5b, the experiment was repeated at an MAS rate of 26 kHz. For both considered proton−proton contacts, the transfer rates, and hence, the 0Q line-shape functions are significantly reduced. Although a direct determination of the 0Q line shape function is difficult, it can be approximated by a product[43] of two 1Q decay functions known to scale with $1/\omega_r$.[44] Hence, the 0Q-line shape function should scale with $1/\omega_r^2$. Indeed, a value of $J^{0Q,LM}(\Delta) = 37\ \mu s$ leads to very good agreement between theory and experimental data for the shorter distance (Figure 5b) and reasonable agreement for the Cβ−Cδ pair. In light of these experimental observations, the assumption of a uniform diffusion constant that is not influenced by the details of the experiment is certainly not justified.

Next we investigated the polarization transfer behavior for different static magnetic fields. In Figure 6, correlations recorded at (a) 9.4 T are compared to data obtained at (b) 14.1 T. Again, uniformly [^{13}C,^{15}N] labeled His·HCl was considered. Apart from the Cδ−Cϵ connectivity, all correlations, including the 3.06 Å (Cβ−Cδ) contact, are characterized by slower build-up rates that increase in intensity beyond the mixing times considered. The relatively fast signal buildup of the Cδ−Cϵ pair in Figure 6a most likely results from relay transfers involving short (^{1}H,^{1}H) distances in the aromatic ring. Remarkably, the theoretical curves (included from Figure 5a) largely describe the buildup characteristics for *both* 400 and 600 MHz NMR data, indicating that the dominating transfer mechanism for proton−proton

(40) Cornilescu, G.; Delaglio, F.; Bax, A. *J. Biomol. NMR* **1999**, *13*, 289−302.
(41) Nilges, M. *Curr. Opin. Struct. Biol.* **1996**, *6*, 617−623.
(42) Hohlwein, D. *Acta Crystallogr. Sect. A* **1977**, *33*, 649−654.

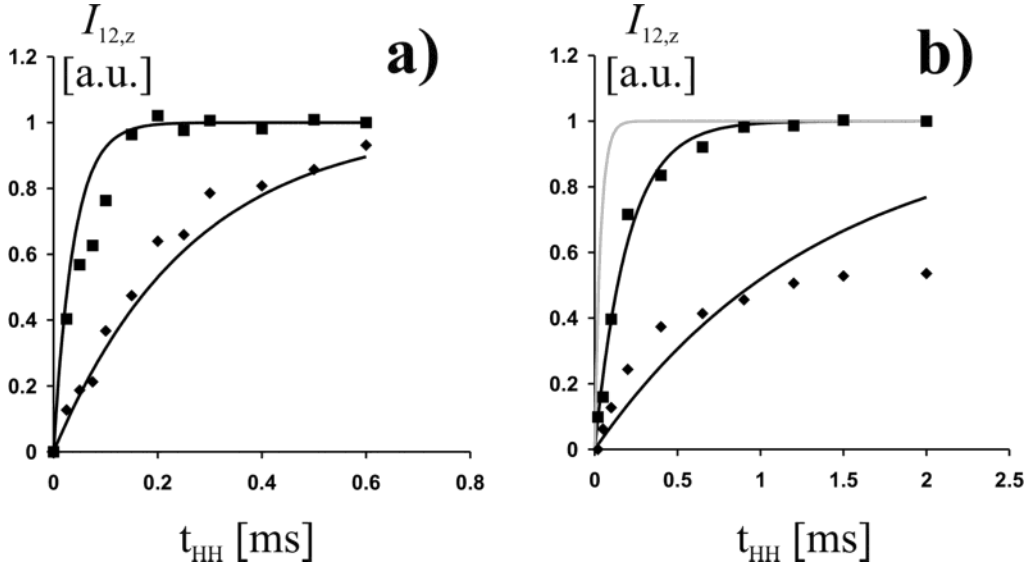

Figure 5. Polarization transfer rates under the LM scheme on U-[^{13}C,^{15}N] labeled His·HCl observed at an MAS rate of 11 kHz (a) and 26 kHz (b). Data sets were calibrated as follows: The observed cross-peak intensities for the C$\alpha-$Cβ (filled squares) and C$\beta-$Cδ (filled diamonds) were normalized against the total intensity of the 2D spectrum. Subsequently, data points for the fastest buildup were set to 1 for long mixing times. Indicated lines correspond to numerical simulations using eq 1, the 0Q line-shape function given in the text and the following simulation parameters: $r_{12} = 2.22$ Å (C$\alpha-$Cβ spin pair) and $r_{12} = 3.06$ Å (C$\beta-$Cδ spin pair). The signal buildup reflects (^{1}H,^{1}H) interactions, encoded in ^{13}C evolution and detection periods. For reference, predictions using $J^{0Q,LM}(\Delta)$ obtained at 11 kHz are included in gray.

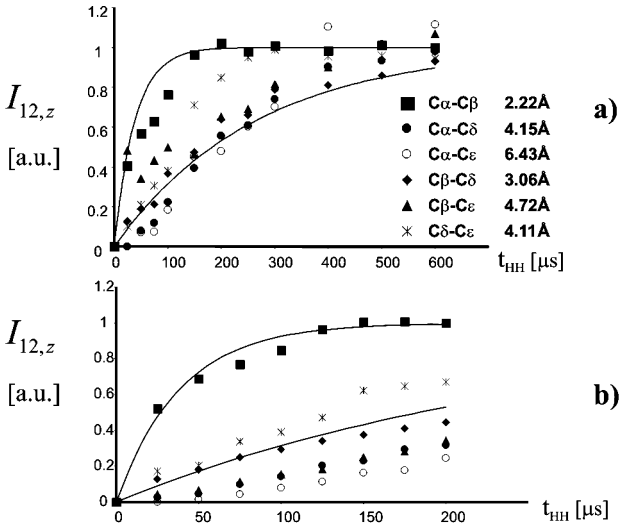

Figure 6. Experimentally observed polarization transfer rates on U-[^{13}C,^{15}N] labeled His·HCl at (a) 400 MHz and (b) 600 MHz under LM mixing. Indicated distances were obtained from previous neutron diffraction studies.[42] Lines correspond to numerical simulations using eq 1 and the following simulation parameters: (a): $r_{12} = 2.22$ Å (C$\alpha-$Cβ spin pair) and, $r_{12} = 3.06$ Å (C$\beta-$Cδ spin pair) and the 0Q-line shape function given in the text. Note that in (b) the time axis is expanded by a factor 3. The signal buildup reflects (^{1}H,^{1}H) interactions, encoded in ^{13}C evolution and detection periods.

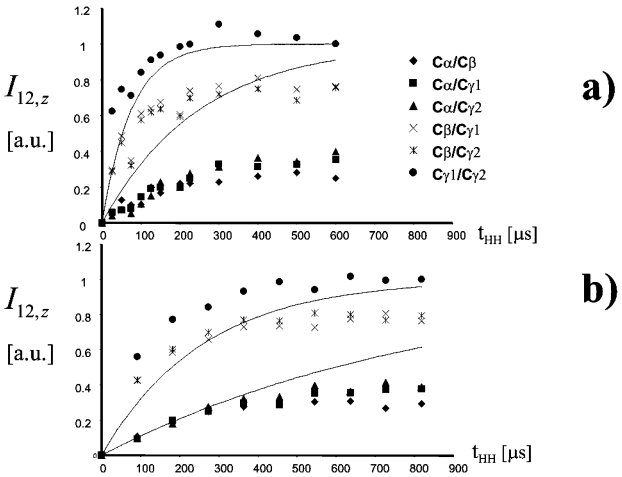

Figure 7. 0Q-CHHC cross-peak buildups in U-[^{13}C,^{15}N] L-valine for longitudinal (a) and RFDR (b) (^{1}H,^{1}H) mixing. Spin pairs are indicated by symbols. Lines correspond to theoretical predictions using the 0Q line-shape function of Figures 5 and 6 and (^{1}H,^{1}H) distances of 2.48 Å and 3.03 Å. Data were obtained on a WB 400 MHz instrument. The signal buildup reflects (^{1}H,^{1}H) interactions, encoded in ^{13}C evolution and detection periods.

distances up to 3Å is only weakly influenced by an increase in isotropic and anisotropic ^{1}H chemical shielding interactions. Apart from a reduction in transfer rates for long distances, the data at higher field strength reveal that the transfer curves do not allow for discrimination between direct contacts and relay mechanisms for distances larger than 3Å. Within experimental error, these buildup rates behave similarly to the 3.06 Å distance predicted for the (C$\delta-$Cβ) pair. As in the solution state, these curves most likely involve relay transfer mechanisms and hence complicate a discrimination between a 3.06 Å (^{1}H,^{1}H) direct contact and multiple-spin transfer mechanism over a comparable length scale. The experimental results obtained using the LM scheme of Figure 3a are hence in qualitative agreement with the theoretical description.

To investigate whether these observations also hold for NMR data obtained in other systems, Figure 7 (a) contains experimental results on U-[^{13}C,^{15}N] variants of L-valine obtained under longitudinal mixing (LM) at 11 kHz MAS. According to the crystal structure,[45] all nearest neighbor (^{1}H,^{1}H) distances are, except for the C$\alpha-$Cβ pair (3.03 Å), identical and short (2.48

(43) Henrichs, P. M.; Linder, M.; Hewitt, J. M. *J. Chem. Phys.* **1986**, *85*, 7077−7086.
(44) Brunner, E.; Freude, D.; Gerstein, B. C.; Pfeifer, H. *J. Magn. Reson.* **1990**, *90*, 90−99; Samoson, A.; Tuherm, T.; Gan, Z. *Solid State Nucl. Magn. Reson.* **2001**, *20*, 130−136.
(45) Torii, K.; Iitaka, Y. *Acta Crystallogr., Sect. B* **1970**, *B 26*, 1317−1319.

Å). Transfer functions assuming the same 0Q line-shape function as in Figure 5a are included for internuclear distances of 2.48 Å and 3.03 Å as reference. An inspection of Figure 7 leads to the following conclusions: (i) the overall intensity of the different spin pairs varies considerably. Because the cross-peak intensities were (as in Figures 5 and 6) normalized against the total intensity of the spectrum, this observation can be partially attributed to intensity variations due to mobility effects. For example, cross-peak amplitudes involving one or two CH_3 groups are in general stronger (Figure 7). (ii) One in general finds cross-peak maxima between 300 and 500 μs consistent with proton−proton distances of about 2.4 Å (vide infra). Correspondingly, a further downscaling of the theoretical curve for the 2.48 Å distance leads to good agreement for the majority of the considered spin pairs. We note that an additional normalization is only justified for buildup curves that display a clear maximum in the considered mixing time regime. (iii) The experimental data do not allow for a reliable detection of the Cα−Cβ distance of 3.03 Å. We attribute this effect to strong relay mechanisms within the highly symmetric arrangement of Val that influence the transfer dynamics for the Cα−Cβ pair. With the exception of this discrepancy, the experimentally observed transfer rates are hence in qualitative agreement with distances obtained from X-ray crystallography. In the solution state, (^{1}H,^{1}H) contacts involving methyl protons are usually described by modified NOE buildup rates.[46,47] Although we did not observe analogous effects in the model systems considered, internal motions could further influence the observed transfer characteristics. Examples involving mobile polymer systems have been reported.[48]

To further investigate the dependence of the transfer dynamics on experimental settings, we have included (Figure 7b) results obtained using RFDR as a (^{1}H,^{1}H) mixing sequence (Figure 3b). Again, the correlation spectra are dominated for short mixing times by the strongest (^{1}H,^{1}H) interactions. RFDR transfer leads, in zeroth order average Hamiltonian theory, to a dipolar Hamiltonian[35] with a recoupling efficiency given by the product of the dipolar coupling element and the (isotropic and anisotropic) ^{1}H chemical shift difference (normalized against the MAS rate) of the two spins of interest. Correspondingly, numerical 2-spin simulations predict (for a proton−proton distance of 2.5 Å) a mixing time dependence that compares favorably to results obtained for one-bond (^{13}C,^{13}C) dipolar recoupling experiments. Instead, the experimental buildup rates shown in Figure 7b are significantly faster and are well described within a monoexponential 0Q-relaxation analysis (eq 1). In agreement with all other correlations, one observes an approximately 3-fold reduction in the polarization transfer rate for the Cγ1−Cγ2 spin pair (filled circles in Figure 7). For the experimental parameters given in Figure 7, we hence find a modified zero-quantum line-shape function. $J^{0Q,RFDR}(\Delta) \cong 0.3J^{0Q,LM}(\Delta)$ favoring the LM approach in practical applications.

The presented results of Figures 5−7 suggest a general approach for the structural analysis of 0Q-CHHC correlation spectra in systems of unknown structure: A semiclassical

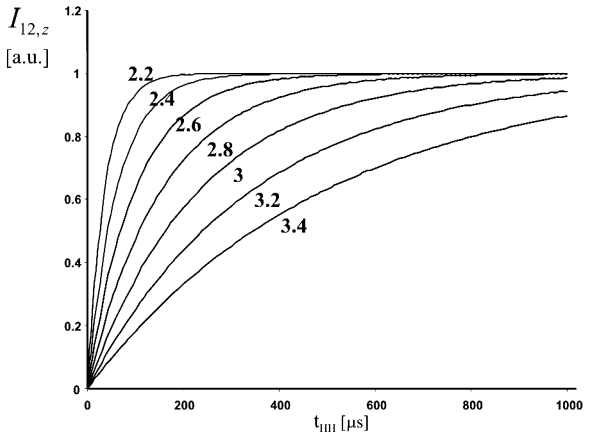

Figure 8. Simplified model describing the initial rate transfer behavior of the 0Q-CHHC LM method. Transverse relaxation rates were selected according to the empirical results obtained in Figures 6 and 7. Assuming the validity of eq 1, these parameters directly correlate with the (^{1}H,^{1}H) distances given in Å. The calibration is valid for experiments at 400 and 600 MHz.

relaxation treatment leads to a uniform zero-quantum line-shape function $\tilde{J}^{0Q}(\Delta)$ for a given MAS rate, 0Q mixing scheme and B_0 field. As exemplified in Figure 8 for the LM scheme and an MAS rate of 11 kHz, one can subsequently construct a transfer map that scales inversely with the 6th power of the internuclear distance. The most reliable structural analysis involves a detailed comparison of the theoretical predictions to the experimentally detected cross-peak buildup intensities. As visible from Figures 5−8, such an analysis permits to detect short (^{1}H,^{1}H) distances with relatively high accuracy (± 0.2 Å) Alternatively, one can solely rely on results obtained for one mixing time in the initial rate regime where the observed signal intensities strongly correlate with the expected proton−proton distance. Similar to the solution state, additional errors due to variations in signal intensity and relay transfer effects must then be taken into account.

We conclude this section by briefly comparing the results regarding 0Q-CHHC mixing to a cross relaxation analysis employed in solution-state NMR. Here, ^{1}H relaxation in the laboratory frame is dominated by dipolar (^{1}H,^{1}H) interactions leading to Nuclear Overhauser effects (NOE) and the rate of polarization transfer between two spins is determined by the Solomon[16] equations. The cross relaxation rate directly depends on the internuclear distance between the two dipolar interacting spins under study and the details of the motional process[15,17] encoded in the generalized spectral density functions $\tilde{J}(\omega_1,\omega_2)$

$$\frac{1}{T^{NOE}} = (\mu_0/4\pi)^2 \frac{\hbar^2 \gamma_I^4}{r_{12}^6} \tilde{J}(\omega_1,\omega_2) \qquad (4)$$

Hence, *both* solid and solution-state rate constants are proportional to $1/r_{12}^6$. Comparison of eq 4 and eq 2 furthermore reveals that the polarization transfer rates in the solid- and liquid-state are determined by multiple-spin and motional effects within a dipolar coupled proton spin network, respectively. As in the solution state, where a significant amount of information is available today regarding the spectral density functions $\tilde{J}(\omega_1,\omega_2)$ for different motional models,[47,49] the presented N/CHHC concept hence allows for a further detailed analysis of the 0Q line shape function under variable experimental conditions and different degrees of proton density and molecular mobility. For

(46) Lane, A. N. *J. Magn. Reson.* **1988**, *78*, 425−439; Olejniczak, E. T. *J. Magn. Reson.* **1989**, *81*, 392−394; Liu, H.; Thomas, P. D.; James, T. L. *J. Magn. Reson.* **1992**, *98*, 163−175.
(47) Koning, T. M. G.; Boelens, R.; Kaptein, R. *J. Magn. Reson.* **1990**, *90*, 111−123.
(48) Fritzhanns, T.; Demco, D. E.; Hafner, S.; Spiess, H. W. *Mol. Phys.* **1999**, *97*, 931−943.

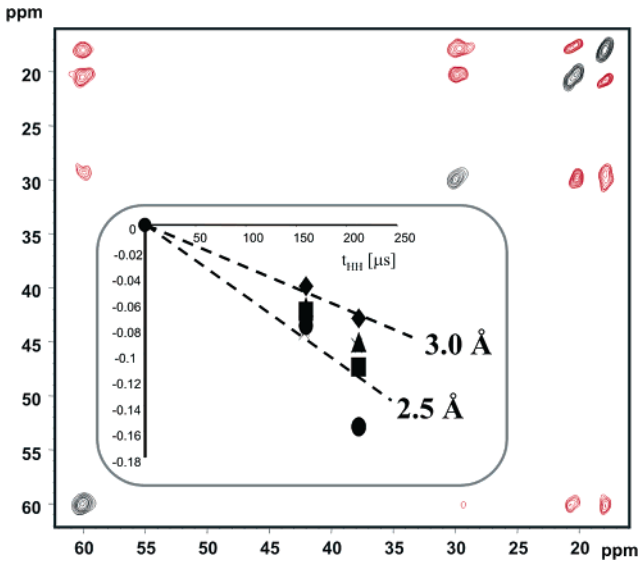

Figure 9. 2Q-CHHC correlation experiment on U-[^{13}C,^{15}N] L-val for t_{CH} = 250 μs and a proton−proton mixing time of 208 μs. Negative signal intensities are given in red. Insert: Symbols (see Figure 7) relate to experimentally detected data points. Dashed lines correspond to initial rate transfer as obtained within a quantum mechanical 2-spin simulation for the designated (^{1}H,^{1}H) distances.

the solid-phase systems considered here, the observed rate constants are about 3 orders of magnitude faster than observed in the solution-state. Additional complications due to scalar couplings[18] can hence safely be neglected.

Double-Quantum (^{1}H,^{1}H) Polarization Transfer. As already demonstrated in ref 26, it is also possible to establish double-quantum polarization transfer in fully protonated systems with transfer characteristics well-known from rare-spin 2Q-correlation experiments. Here, a 0Q-spin diffusion approximation does not adequately describe our experimental findings. Instead, QM two-spin simulations were conducted for variable MAS rates indicating that POST-C7 dipolar recoupling is possible at 11 kHz for (^{1}H,^{1}H) distances equal to or longer than 2.0 Å. At higher spinning speeds, stronger dipolar couplings and hence proton−proton distances down to 1.5 Å can be investigated.

Figure 9 contains experimental results obtained on U-[^{13}C,^{15}N] L-valine for a homonuclear contact time of 208 μs. As expected,[50] all cross-peak intensities are negative relative to the positive signal values of the diagonal. In agreement with the crystallographic predictions (see previous section), the cross-peak amplitudes involving the (Cα−Cβ) spin pair are considerably smaller than all other cross-peak intensities observed in the spectrum. We can compare the cross-peak buildup rates in the initial rate regime to quantum mechanical two-spin simulations for internuclear (^{1}H,^{1}H) distances of 2.5 Å and 3.0 Å. The corresponding initial linear transfer rates are indicated in Figure 9 as dashed lines. The NMR data are hence in good agreement with the X-ray structure. For short mixing times, (i.e., $t_{HH} \leq$ 0.2 ms), the size of the 2Q cross-peak intensity reflects the internuclear (^{1}H,^{1}H) distance. For longer mixing times, strongly coupled systems require the inclusion of further proton spins within the simulation and the observed transfer amplitude changes sign in close analogy to the (^{13}C,^{13}C) case.[51] These experimental observations are in full agreement with additional three-spin model calculations (data not shown) and reveal that relay mechanisms dominate the transfer behavior for longer mixing times. According to these calculations, increasing the MAS rate does not alter the transfer dynamics for distances between 2 Å and 4 Å but enables the detection of shorter proton−proton distances.

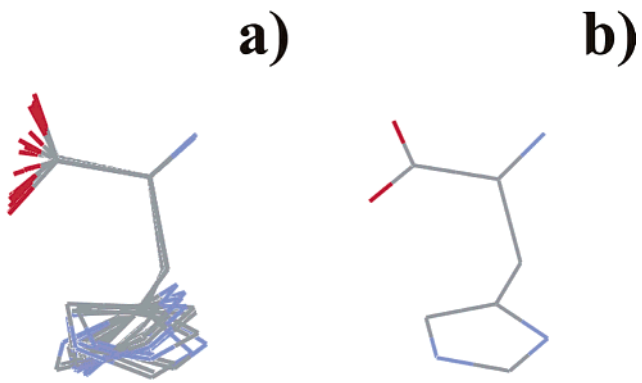

Figure 10. Comparison of (a) a representative ensemble of 10 structures of His·HCl using 0Q-CHHC constraints with (b) the published conformation obtained from neutron diffraction.[42] The structures were aligned along all heavy atoms excluding oxygen and aromatic ring atoms using MOLMOL.[58]

(B) 3D Structure Determination using (^{1}H,^{1}H) Restraints. In the following, we exemplify in two simple cases how the structural constraints obtained from N/CHHC correlation spectra can be used in the context of a standard three-dimensional structure determination. In both cases, uniformly labeled samples were considered within an unlabeled background hence excluding contributions from intermolecular (^{1}H,^{1}H) transfer. Such interactions can provide valuable structural information but would complicate the interpretation of the transfer dynamics in terms of the 3D molecular structure. For sensitivity reasons,[26] we here concentrate on results using the 0Q-N/CHHC LM method.

L-**His·HCl.** As a cross validation, the CHHC data shown in Figure 6 were used to establish a set of structural constraints for L-His·HCl. On the basis of the analysis presented in (A), we assumed distance restraints [r_{ij}^l, r_{ij}^u] of [1.8 Å, 2.3 Å] for the (Cα−Cβ) pair and [2.6 Å, 10 Å] for all other considered (^{1}H,^{1}H) contacts. The 10 lowest-energy structures shown in Figure 10a were hence obtained using in total 6 nontrivial (^{1}H,^{1}H) distance constraints. The agreement to the conformation obtained from neutron diffraction[42] (Figure 10b) could be further improved by a detailed analysis of 2Q-CHHC experiments that allow for a clear distinction between direct and relay mechanisms.

Ala-Gly-Gly. To assess the usefulness of the presented approach in peptides, we next considered NMR results obtained on the uniformly [^{13}C,^{15}N] labeled tripeptide Ala-Gly-Gly for which a crystallographic reference structure is available.[52] In addition to the CHHC-type of experiments we here also recorded a series of NHHC correlation experiments. As an example, Figure 11 contains results of a LM 2D experiment with t_{HH} =

(49) Noggle, J. H.; Schirmer, R. E. *The Nuclear Overhauser Effect*; Academic Press: New York and London, 1971; Massefski, W.; Bolton, P. H. *J. Magn. Reson.* **1985**, *65*, 526−530; Neuhaus, D.; Williamson, M. *The Nuclear Overhauser Effect in Structural and Conformational Analysis*; VCH Publishers: New York, Weinheim, Cambridge, 1989.
(50) Baldus, M.; Tomaselli, M.; Meier, B. H.; Ernst, R. R. *Chem. Phys. Lett.* **1994**, *230*, 329−336.
(51) Sun, B. Q.; Costa, P. R.; Kocisko, D.; Lansbury, P. T.; Griffin, R. G. *J. Chem. Phys.* **1995**, *102*, 702−707.
(52) Subramanian, E., Lalitha, V. *Biopolymers* **1983**, *22*, 833−838.

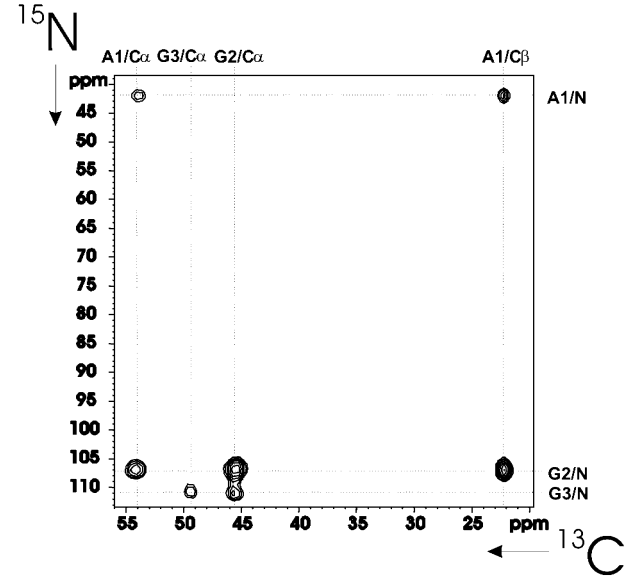

Figure 11. 0Q-NHHC correlation experiment on 3 mg of U-[^{13}C,^{15}N] AGG for a LM correlation time of 200 μs. The experiment was conducted at 9.4 T and 11 kHz MAS. t_{NH} was set to 500 μs. Resonance assignments were obtained from ref 30. All peaks reflect (^{1}H,^{1}H) interactions, encoded in ^{15}N evolution and ^{13}C detection periods.

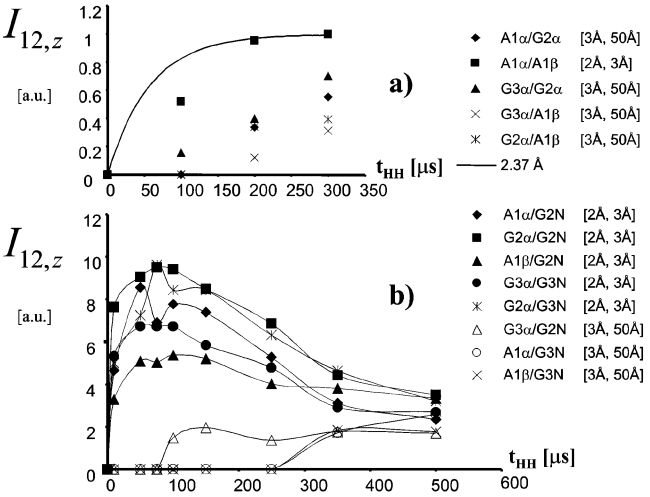

Figure 12. (a) CHHC buildup curves for the indicated cross-peaks. The solid line corresponds to a theoretical prediction (see Figure 8) using a (^{1}H,^{1}H) distance of 2.37 Å, (b) 0Q-NHHC signal buildup for the indicated (N,C) pairs. For the sake of clarification, connecting lines are shown. All experiments were conducted using the LM scheme (Figure 3a) on 3 mg of U-[^{13}C,^{15}N] AGG at 11 kHz MAS and 400 MHz (^{1}H resonance frequency). Resonance assignments were obtained from ref 30. Distance restraints used during the structure calculations are indicated.

200 μs. Again, only protonated rare-spins are considered, and it is hence sufficient to concentrate on the aliphatic region of the spectrum. Similar to the homonuclear CHHC case, one immediately observes significant differences regarding the intensity of the observed correlations. These qualitative observations are supported by an analysis of the resulting CHHC (a) and NHHC (b) buildup curves on AGG shown in Figure 12.

From the CHHC data presented in (a), we can easily identify one short (^{1}H,^{1}H) distance for the (A1Cα, A1Cβ) pair. Notably, the initial rate buildup agrees well with a theoretical approximation of Figure 8 assuming the (^{1}H,^{1}H) distance of the corresponding X-ray structure. In contrast to the CHHC correlations, we detect in Figure 12b local maxima for all, according to the X-ray structure, short (i.e., 2.6 Å $\pm$ 0.25 Å) NHHC correlations. For longer mixing times, all signal intensities adopt similar values. The qualitative difference between NHHC and CHHC spectra most likely results from a different degree of total ^{1}H polarization in the sample. In (b) only, NH protons are initially polarized and magnetization must be redistributed within the protonated ^{13}C network. As a result, transfer to nearest neighbor ^{13}C is influenced by other protons in close spatial proximity. These experimental results are in qualitative agreement with quantum-mechanical calculations of an IS_2 spin system.[7] Comparison of Figure 11 and Figure 12 indicates that one 2D correlation experiment is sufficient to identify nearest neighbor NHHC correlations. Two of the detected interresidue correlations involve Cα(i)$-$NH(i+1) pairs strongly indicative[13] for a β -strand arrangement of AGG predicted from the crystal structure. In a simplified, dual constraint classification, we can attribute strong peaks in Figure 11 to NHHC distances of [2.0 Å, 3.0 Å] and all other weak or missing correlations to (^{1}H,^{1}H) distances of [3.0 Å, 50.0 Å]. Similar to the study involving L-His·HCl, selecting a large upper structural bound appropriately reflects the accurateness of the NMR-detected distance constraints and minimizes complications due to relay effects during the structure calculation. Note that in contrast to approaches involving chemical-shift-selective transfer methods, 12 nontrivial distance constraints were hence obtained from a *single* 2D experiment.

These distance constraints can provide the basis for the computation of an ensemble of 3D structures. In addition to these distances constraints, secondary chemical shifts strongly correlate with polypeptide backbone structure[30,53] and provide a convenient means for establishing dihedral angle constraints in a polypeptide.[5,40,54] In particular, we have recently shown that solution-state random coil chemical shifts can be used as a standard reference to study secondary chemical shifts of uniformly labeled proteins in the solid-state.[30] As a result, databases such as the TALOS[40] routine, originally developed for the structural analysis of conformation-dependent chemical shifts in the solution-state, can be used for solid-state NMR applications.[3,9,54,55] In the case of AGG, we find for the central residue of AGG ($\phi = (-104 \pm 23)°$, $\psi = (158 \pm 24)°$) which is in reasonable agreement with the X-ray structure and provides an independent additional structural constraint. For the particular case of AGG, a structure calculation with CNS using *only* these dihedral angle constraints leads to the structure shown in Figure 13a and a backbone RMSD of 0.51 Å. As expected, C and N terminal segments of the peptide remain poorly defined and additional constraints are necessary. In Figure 13b, NHHC distance parameters were supplemented as additional constraints leading to an overall reduction of the backbone RMSD to 0.37 Å. Restraints derived from the NHHC correlation experiment are particularly useful to restrict the N terminus and the side chain. On the other hand, the C-terminus remains, in the absence of detectable (^{1}H,^{1}H) contacts, poorly defined. Correspondingly, the beneficial effect of the (^{1}H,^{1}H) constraints becomes apparent

(53) Saito, H. *Magn. Reson. Chem.* **1986**, *24*, 835−852; Spera, S.; Bax, A. *J. Am. Chem. Soc.* **1991**, *113*, 5490−5492; Dedios, A. C.; Pearson, J. G.; Oldfield, E. *Science* **1993**, *260*, 1491−1496.
(54) Balbach, J. J.; Ishii, Y.; Antzutkin, O. N.; Leapman, R. D.; Rizzo, N. W.; Dyda, F.; Reed, J.; Tycko, R. *Biochemistry* **2000**, *39*, 13 748−13 759.
(55) Ishii, Y. *J. Chem. Phys.* **2001**, *114*, 8473−8483; Böckmann, A.; Lange, A.; Galinier, A.; Luca, S.; Giraud, N.; Heise, H.; Juy, M.; Montserret, R.; Penin, F.; Baldus, M. *J. Biomol. NMR* **2003**, in press.

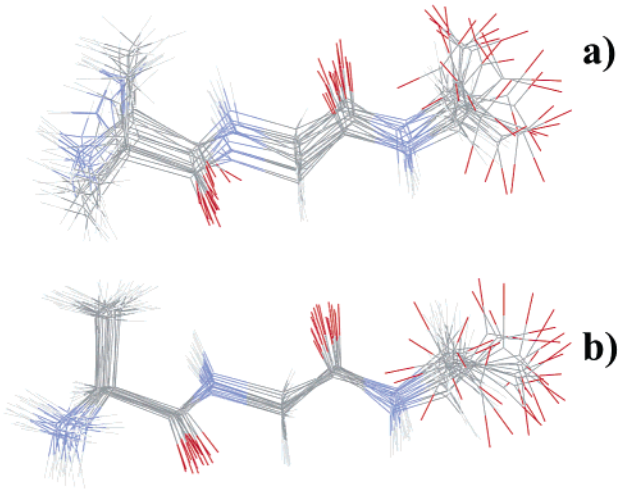

Figure 13. Representative ensemble of 20 structures of AGG using (a) TALOS dihedral angle constraints only and (b) their combination with NHHC distance constraints. The structures were aligned along the backbone atoms of all three residues using MOLMOL.[58]

when RMSD values are calculated without the C terminal C′ atom. In this case, the RMSD value decreases from 0.39 Å (TALOS) to 0.17 Å (TALOS + NHHC). Hence, the combination of the ^{13}C resonance assignments and a single NHHC experiment was sufficient to significantly restrain the 3D structure of AGG in the solid state. Because only one side chain resonance can be detected, CHHC distance constraints do, in the current context, not lead to significant increase in structural accuracy.

Conclusions

The detection of through-space contacts represents one of the primary instruments of NMR to probe structural parameters in solution or solid state. In many applications of chemical or biological relevance, the system of interest is characterized by a large number of proton−proton contacts that, in contrast to rare-spin interactions, are indicative of the three-dimensional arrangement of the molecule of interest. In the solution state, these contacts are easily detected by direct (^1H,^1H) correlation experiments and have been of central importance for 3D structure determination. Both aspects provide a strong incentive to investigate whether a similar approach is viable for the structural analysis of solid biomolecules studied under high-resolution solid-state NMR conditions.

Although we[26] and others[56] have recently demonstrated that N/CHHC experiments can provide structural constraints in polypeptides and proteins, a general approach on how to analyze proton−proton contacts in terms of internuclear distances has thus far not been presented. As confirmed in the first part of our contribution, this aspect may partially be attributed to the fact that an appropriate theoretical description of (^1H,^1H) transfer rates generally depends on the details of the NMR experiment. Our study in model compounds suggests a general framework in which (^1H,^1H) transfer rates can be related to internuclear distances for a given MAS rate and proton−proton mixing scheme.

For the two considered zero-quantum polarization transfer schemes, the spin system dynamics are well described within a semiclassical relaxation theory and lead to an exponential cross-peak buildup. For a given MAS rate and pulse scheme considered here, a uniform 0Q-line shape function can be obtained and the 0Q-transfer rates depend on the inverse 6^{th} power of the proton−proton distance. For 0Q-NHHC mixing, multiple-spin effects affect the transfer profile for longer mixing times. Nevertheless, the initial transfer rate remains diagnostic for the NHHC distance of interest. The same observations were made for 2Q rotating frame mixing where the initial cross-peak buildup is again sensitive to the internuclear distance and can be described within a quantum-mechanical two-spin analysis. In several aspects, the approach resembles a structural analysis of NOE parameters in the solution state:[57] The accuracy with which proton−proton contacts can be related to internuclear distances is highest if results of several experiments are analyzed in the initial rate regime. Relay transfers and intensity variations can be accounted for by choosing appropriately wide bounds or by a direct refinement during the structure calculation.[41] Finally, 2Q-CHHC correlation spectra can, similar to ROESY experiments, help to distinguish direct from relay transfer. Hence, the presented concept should be of comparable value to NOE-related spectroscopy in the solution-state.

In two simple examples, we have shown how (^1H,^1H) constraints can be used to determine molecular structures using solid-state NMR. In contrast to previous reports, a small set of 2D experiments was sufficient to establish side chain or backbone conformation in two model systems. For AGG, a single NHHC correlation spectrum suffices to calculate the 3D structure to a backbone RMSD of 0.37Å. Our investigation provides the empirical basis for future structural studies in other protonated molecules including ligands of small molecular weight,[3] fibrous or membrane proteins. Here, (^1H,^1H) contacts not only report on local backbone or side chain orientation but they are particularly useful to establish medium and long-range constraints for the three-dimensional protein fold. We have previously shown for the 76 residue protein ubiquitin that such constraints can in principle be detected using the discussed N/CHHC concept.[26] Provided that a sufficient number of proton−proton distances and dihedral angle constraints can be obtained, solid-state NMR experiments as discussed here could hence lead to the de novo protein structure determination using a single protein sample.

Acknowledgment. Scientific discussions with Prof. Dieter Suter (University of Dortmund), Prof. Christian Griesinger, Dr. Henrike Heise, and Dr. Colan Hughes are gratefully acknowledged. This study has been funded in part by a Ph.D. fellowship to A.L. from the Stiftung Stipendien-Fonds of the Verband der Chemischen Industrie and an Alexander von Humboldt postdoc fellowship to L.V.

Supporting Information Available: Additional details regarding the quantum-mechanical two-spin calculations used in Figure 2 and Figure 9. This material is available free of charge via the Internet at http://pubs.acs.org.

JA034555G

(56) Tycko, R.; Ishii, Y. *J. Am. Chem. Soc.* **2003**, *125*, 6606−6607.
(57) Nilges, M. *Fold. Des.* **1997**, *2*, S53−S57.
(58) Koradi, R.; Billeter, M.; Wuthrich, K. *J. Mol. Graph.* **1996**, *14*, 51−60.